Gas Slit Camera (GSC) on MAXI

Tatehiro Mihara,[1] and the MAXI team

[1] MAXI team, RIKEN, 2-1 Hirosawa, Wako, Saitama, Japan 351-0198
E-mail(TM): tmihara@riken.jp

Abstract

The Gas Slit Camera (GSC) is the main instrument of the Monitor of All-sky X-ray Image (MAXI) mission on the International Space Station. The GSC scans the entire sky in every 92-minute orbital period in the 2–30 keV band and achieves the highest sensitivity among the X-ray all-sky monitors. The GSC employs large-area position-sensitive proportional counters with the total detector area of 5350 cm^2. We describe the instruments, on-board data processing, and performance in the ground calibration experiment.

Key words: instrumentation: detectors — MAXI – GSC — proportinal counters

1. Introduction

Monitor of All-sky X-ray Image (MAXI) (Matsuoka et al. 2009) is a mission onboard Japanese Experimental Module - Exposed Facility (JEM-EF) on the International Space Station (ISS). MAXI carries two kinds of X-ray cameras : Gas Slit Camera (GSC: Mihara et al. 2011; Sugizaki et al. 2011) and Solid-state Slit Camera (SSC: Tsunemi et al. 2010; Tomida et al. 2011). Both GSC and SSC employ slit and collimator optics. The GSC consists of twelve identical units, and the SSC consists of two. The payload was launched by the space shuttle Endevour on July 16, 2009, then mounted on the port No. 1 on JEM-EF on July 24. After the electric power was turned-on on August 3, MAXI started nominal observation since August 15, 2009.

2. Camera Design

The MAXI/GSC employs the slit camera optics. The slit camera has an advantage of being free from the source contamination over the coded-aperture mask while it has a disadvantage in the limited slit area. Thus, it is better suited for relatively faint and stable sources such as AGNs. To achieve the high sensitivity, large-area proportional counters filled with Xe gas are used for the X-ray detectors. The total detector area of 5350 cm^2 using twelve gas counters is optimized within the limit of the payload size ($0.8\times1.2\times1.8$ m^3).

The position-sensitive proportional counter resolves the incident direction from the projected slit image. In the slit camera, one point of the sky always corresponds to only one point on the detector (1:1). The background subtraction is simple and we can easily accumulate many scans up to years, which leads the high-statistics data. On the other hand in the coded mask, the instant effective area for one source is larger. However, many points of the sky affects the count-rate of one point on the detector (many:1). The error of a source count-rate is enlarged by a stronger sources in the FOV. The background for the source is not stable in the coded mask. The summation for years and spectral analysis of each source in the same FOV are not trivial.

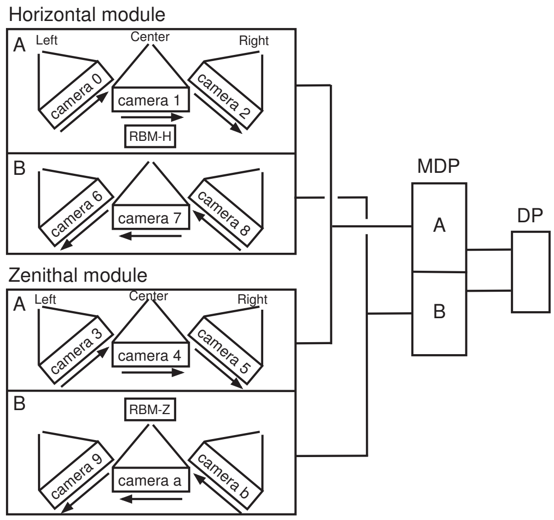

Fig. 1. Schematic drawing of GSC cameras. The camera numbers are marked in hexadecimal as 0...9, a and b. Six cameras are assembled into two modules whose field of views are aimed to the horizontal/zenithal directions in orbit. Two cameras in each direction are connected to the two individual readout systems (MDP-A/B) independently for the redundancy. The arrow in each counter indicates the X direction (DETX) of carbon anodes. Two RBM (Radiation-Belt Monitor) detectors are mounted in the middle of the central cameras of both the horizon and the zenith modules.

Figure 1 illustrates the schematic drawing of the GSC camera units on the MAXI payload. The entire GSC systems are composed of six identical units. Each unit

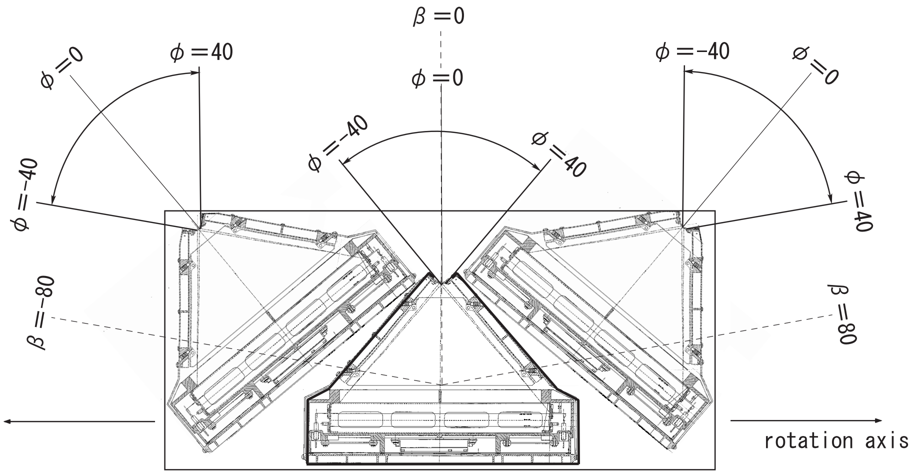

Fig. 2. Cross-section view of each horizon/zenith module. Three camera units are packed in a rectangular space. The incident angle ϕ is defined for each camera, while the source-acquisition angle β is defined for the MAXI payload. The thick outline on the center camera indicates the shields made of 0.1-mm lead and 0.1-mm tin sheets installed to block external X-ray.

consists of a slit and slat collimator and two proportional counters with one-dimensional position-sensitivity. The two counters in each unit are controlled by two individual data processors (GSC MDP-A/B) via independent signal paths for the redundancy.

The six camera units are assembled into two groups whose field of views (FOVs) are pointed toward the tangential direction of the ISS motion along the earth horizon and the zenith direction. They are named as horizon and zenith modules respectively. Each horizon/zenith module covers a wide rectangular FOV of $160^\circ \times 1.5^\circ$ (FWHM) with an almost equal geometrical area of 10–20 cm^2 combining three camera units. Figure 2 shows the cross-section view of each module. The areas of 10° from the FOV edges to both the rotation poles are not covered because these directions are always obstructed by the ISS structures.

The two FOVs of the horizon and the zenith modules both scan the almost entire sky in the 92 minutes orbital period. Any X-ray source is, therefore, observed twice in a orbit. The horizon module precedes the zenith module by 21.5 minutes in the normal ISS attitude. The FOV of the horizon unit is tilted up by 6 degree above the direction of the ISS motion to avoid the earth atmosphere as an allowance for the possible ISS attitude fluctuation. The FOV of zenith units is set in the plane that includes the zenith and is perpendicular to the direction of motion. Both FOVs have no earth occultation and use no moving mechanics. The two FOVs are capable of covering the whole sky even if some of the counters have to be suspended from operation. The sampling period of 92 minutes is suited to the studies of long-term variability ($>$ 1 hour) such as AGNs.

3. Detector Unit

3.1. Gas counter

The GSC proportional counters employ resistive carbon fibers with a diameter of 10 μm for anode wires. Higher resistive anodes are preferable for the better position resolution because the thermal noise on the readout signal is inversely proportional to the anode resistance. A carbon fiber is better than a nichrome wire in this point. Although the traditional carbon-coated quartz has a larger resistance, it is mechanically weak, thus easy to break by launch vibration. The carbon fiber anodes in the GSC were developed at RIKEN and were successfully used in the HETE/WXM (Shirasaki et al. 2003).

Figure 3 shows a picture of a single GSC proportional counter. All the flight counters were manufactured by Metorex (now a part of Oxford Instruments) in Finland. The front X-ray window has an area of 192 $\times$ 272 mm^2. It is sealed with a 100-μm-thick beryllium foil. To support the pressure on the beryllium foil in vacuum that amounts 740 kgW in the whole area, grid structures with a 17-mm height are placed every 10.6-mm pitch parallel to the anode wires. The maximum pressure of 1.66 atm is expected at the temperature of 50°C. Every flight counter was tested to withstand 1.5 times higher than the design pressure, i.e. 2.5 atm. The bodies of the gas counters were made of titanium, which has sufficient strength and a heat expansion coefficient close enough to that of beryllium.

Figure 4 and 5 show the counter cross-section views. The gas cell is divided by ground wires into six carbon-anode cells for X-ray detection and ten tungsten-anode cells for particle veto. The carbon-anode layer and the bottom veto-detector layer have depths of 25 mm and

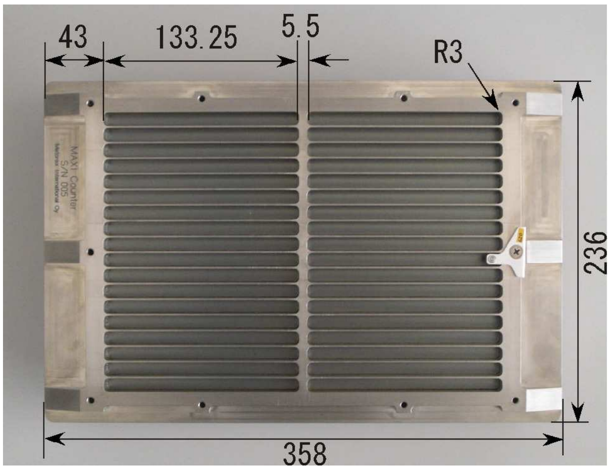

Fig. 3. GSC proportional counter in top view. Numbers are in units of mm. The size of the counter is 358 × 236 × 86 mm^3. The window is sealed with 100-μm-thick beryllium foil, which is supported by the beams of a 17-mm height and a 1.4-mm width placed every 10.6-mm pitch and a think center beam of a 5.5-mm width. The carbon-anode cell is 32 mm in width or for three narrow windows.

18 mm, respectively. These sizes are determined so that the main X-ray detectors and the veto detectors have enough efficiencies for X-rays in the 2–30 keV band and minimum-ionization particles, respectively. The minimum-ionization energy in the 18-mm thick Xe gas is 30 keV. The carbon anodes and veto anodes are not located at the center of each cell in the vertical direction. The anode locations, the aspect ratios of these gas cells, and the spacings of the ground wires are determined so that the spatial non-uniformity of gas gain is small within each cell.

The tension of the carbon-anode wire is set to 4 gW, which is sufficiently smaller than the breakage limit, ~ 25 gW. All anode and ground wires are fixed via a spring at right end to absorb the difference of the heat expansion coefficient and keep the wires tight and straight. The veto anode wires are made of gold-coated tungsten with a 18-μm diameter, which is pulled with a tension of 18 gW. We chose as thin wires as possible for veto anodes to achieve similarly high gas gain as the carbon anodes since the same high voltage (HV) is applied to both the carbon anodes and the veto anodes. The gas-gain ratio of carbon anode to the veto anode is 20:1. The ground wires are made of gold-coated tungsten with a 50 μm diameter. The tension is about 50 gW.

We tested several kinds of gas mixture and chose a combination of Xe (99%) + CO_2 (1%) with a pressure of 1.4 atm at 0°C. The amount of CO_2 is decreased from WXM PC (3%) (Shirasaki et al. 2003) in order to reduce the spatial gas-gain non-uniformity (section 4.3.), and still keep the sufficient quenching effect (Mihara et al. 2002).

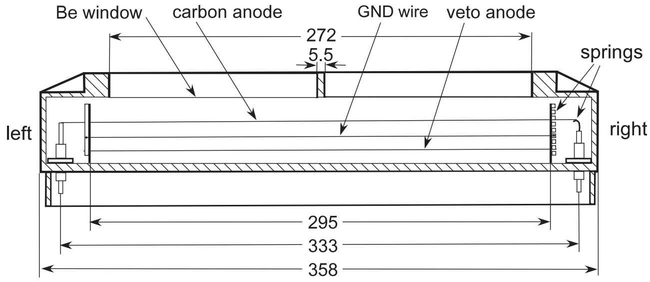

Fig. 4. Cross-section view of GSC proportional counter along the wire direction. Numbers are in units of mm.

The position resolution and the energy resolution are incompatible requirements. The position resolution is primarily determined by the thermal noise on the resistive-anode wire against the readout signal charge. The higher gas gain is basically preferred for the better position resolution. However, the high voltage for the best position resolution is usually in the limited proportionality region rather than the proportionality range, where the spatial gain non-uniformity is larger due to the space-charge effect, which also degrades the energy resolution. The operating high voltage (HV = 1650 V and the gas gain of 7,000) is chosen to achieve a sufficient position resolution and still keep an adequate energy resolution.

For the in-orbit calibration, a weak radioactive isotope of ^{55}Fe is installed in every counter, which illuminates a small spot of about 1 mm in diameter at the right end of the C2-anode cell (figure 3 and 5). Each isotope has a radiation of 30 kBq and its count rate by a GSC counter is about 0.2 c s^{-1} at the launch time.

3.2. Front-end electronics

Each GSC counter has six position-sensitive anodes readout at the both ends (left and right), and two signals for connected veto anodes. A total 14 preamplifiers are used for the 14 analog signals.

The front-end electronics boards are built in the backside of the proportional counter. It is designed to shield external noises and also to strengthen the counter frame. The electronics boards include the high-voltage power supply, HK (House-Keeping) electronics and their connectors. The HK circuit monitors temperatures at eight points in the camera (HV box, preamplifiers, gas cell, etc.) and HV values. The HV-power supply with a low-power consumption was manufactured by Meisei Electric Co. Ltd. Figure 6 illustrates the configuration of the HV connections in each counter. One HV-power-supply unit works on one GSC counter. In total, twelve HV-power-supplies are used. The coupling capacitors connecting the preamplifiers and the anode wires are of 2200 pF, which have sufficiently lower impedance (< 1 kΩ for 2μs

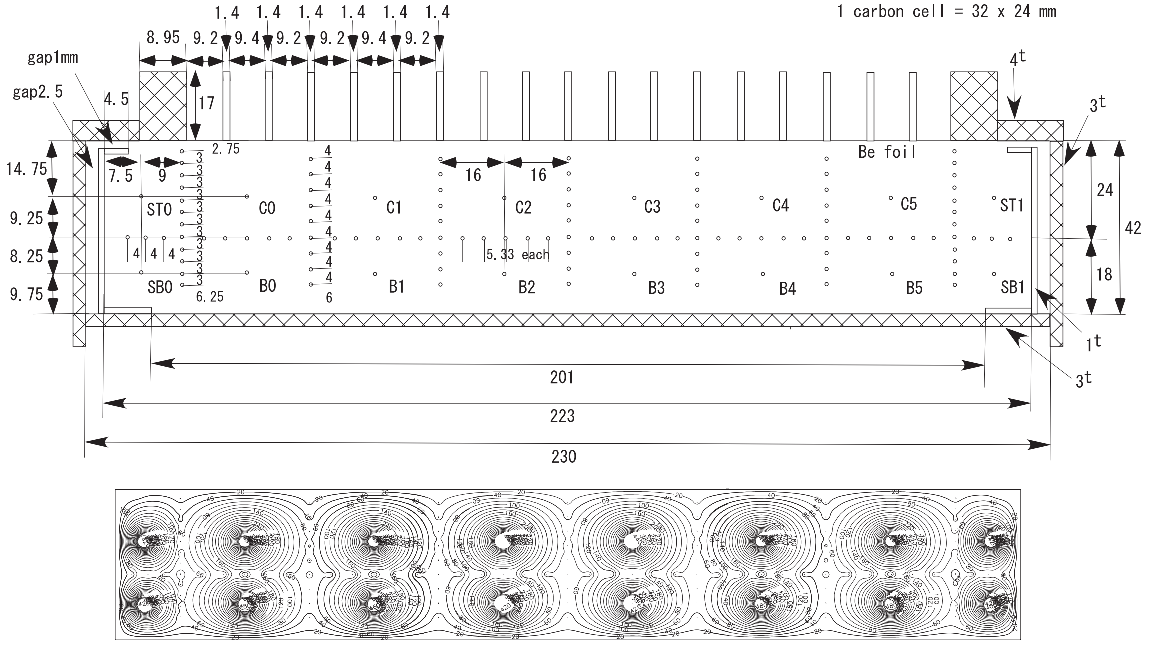

Fig. 5. Cross-section view of GSC proportional counter on the plane perpendicular to the anode wires. All anode/ground-wire locations are shown. The names for anode, C, B, ST and SB, denote Carbon, Bottom, Side Top and Side Bottom, respectively. The wires of B0 to B5 are connected together in the counter and read out as a single bottom-veto (BV) signal. The same for ST0, ST1, SB0 and SB1, as a side-veto (SV) signal. All numbers represent the scale in units of mm. Electric potential in the counter calculated by Garfield is shown in the below. The "Garfield" is a program to simulate gas counters developed in CERN (http://garfield.web.cern.ch/garfield/).

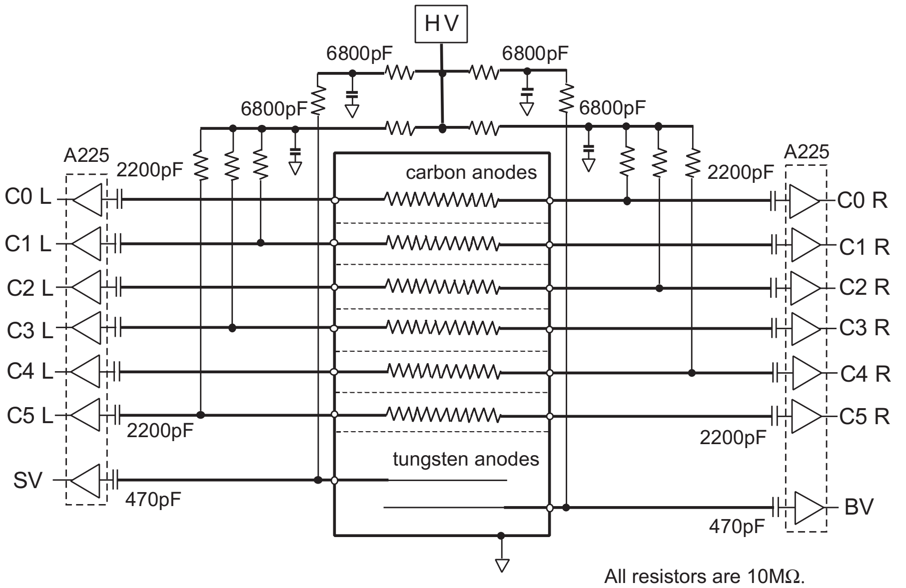

Fig. 6. Schematic view of high-voltage connections to anode wires on the front-end circuit board.

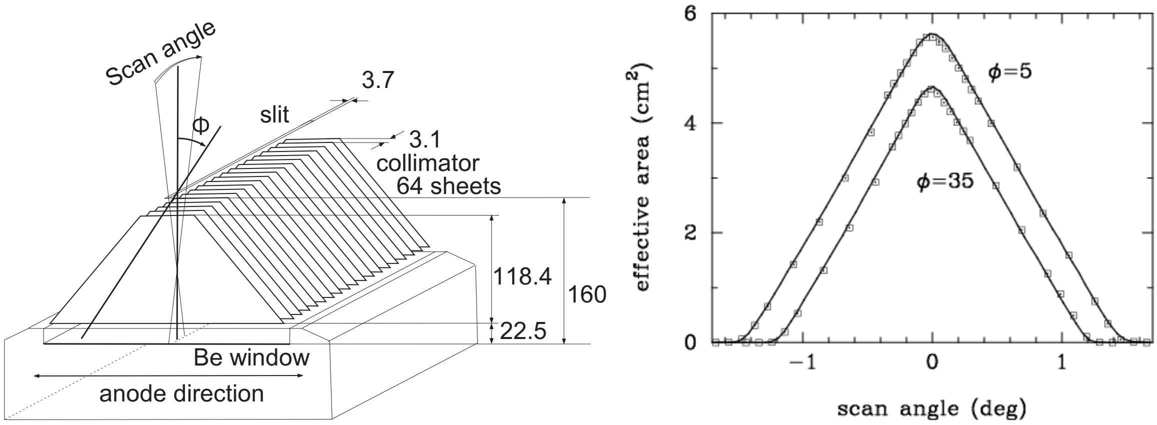

Fig. 7. (Left): Geometry of GSC slit and slat collimator. All numbers represent the scales in units of mm. Collimator sheets are 0.1-mm thick and placed by 3.1-mm pitch. (Right): Effective area of slit and slat collimator for $\phi = 5°$, $35°$. Points represent data measured with X-rays at Cu-K line (8.0 keV) in a ground test and solid lines represent the response models constructed for the data.

shaping out signal of the preamplifier) than that of the carbon anodes (33 kΩ) and still do not accumulate too much charge for the preamplifiers.

Since the wire hermetic rods come out from both the anode ends, two front-end circuit boards are placed separately at the side ends. We selected a hybrid-IC, Amptek A225, for the preamplifier, which is made with a space-use quality and has a low-power consumption.

The preamplifier gains represented by the ratio of the output pulse height to the input charge (Volt/Coulomb) should be the same between the left and the right of each carbon anode. We thus measured gains of all A225 chips under the temperature condition of -20 to $60°$C, then selected pairs whose gains show a similar temperature dependence. The feedback capacities of veto anodes are left as they are 1 pF at the default, while those of carbon anodes are modified to 4 pF by adding an external 3 pF capacitor in order to obtain closer pulse heights for both signals from carbon anodes and veto anodes. The ratio becomes 5:1.

3.3. Slit and Slat Collimator

Figure 7 illustrates the schematic view of the GSC slit and slat collimator. The parallel tungsten rods with 3.7-mm separation are placed at the top of the slat collimator constituting the opening slit of the camera. The collimator slats with a 118.4-mm height, placed at 3.1-mm pitch, constitute the FOV of 1.5° in FWHM, which are aligned vertically to the slit rods. The slats are made of phosphor bronze with 0.1 mm thick. The thickness is determined so that X-rays up to 30 keV are stopped and the sheets can be flattened when pulled by the tension springs. These surfaces are chemical-etched and roughened to avoid reflection. 64 slats are installed at the front of each counter. The "roofs" of the collimator module (as shown in a thick outline in Figure 2) and the both ends of slat collimators are covered by 0.1-mm lead and 0.1-mm tin sheets to shield Cosmic X-ray Background (CXB). Twice thicker shield made of 0.3-mm lead and 0.1-mm tin sheets are placed to block the direct path from the space to the beryllium window.

The collimator transmission was tested in the JAXA beam facility. The setup of ground calibration is described in Morii et al. (2006). The transmissions are confirmed to be within ±5 % of the design. A model of the transmission function was constructed based on the measured data. Figure 7 right panel shows a comparison between the measured data and the model. The in-orbit alignment calibration was carried out using celestial X-ray sources, Sco X-1 and the Crab nebula, and is described in Morii et al. (2011).

4. Detector performance

4.1. Energy Band and Efficiency

The efficiency curve is shown in figure 5 in Matsuoka et al. (2009). It stays higher than 15% in the GSC nominal energy range of 2–30 keV. In the lower energy end, the efficiency drops due to the absorption in the 100-μm-thick beryllium window and varies from 2 to 5% at 1.5 keV according to the X-ray incident angle of 0°–40°. In the higher energy range, the efficiency jumps up at the Xe K-edge energy of 34.6 keV by a factor of 4.8. X-ray events whose energy is higher than the K-edge lose K-line energy due to the escape of fluorescence lines. The escape probability of Xe K-line is 66%, thus it has a significant effect on the counter response. We measured the escape fraction and the complex energy response around the Xe K-edge energy using GSC flight-spare counter at KEK photon factory.

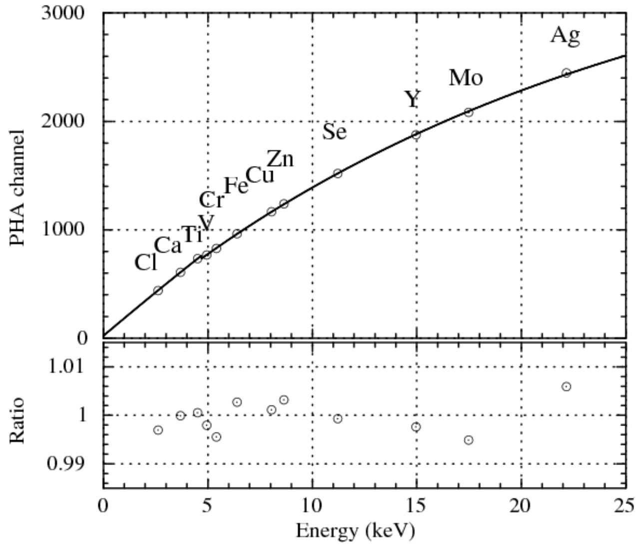

Fig. 8. Linearity of energy-PHA (Pulse height amplitude) relation. Circles represent measured data for K-shell emission lines from the elements labeled. The data were taken with pencil X-ray beams irradiated at an off-wire position of counter #0 anode C0 in the nominal HV of 1650 V. Bottom panel shows residuals from a model expressed by expedient function, $a - b\exp(cE)$. The discontinuity at the Xe L-edge (4.70 keV) is implemented in the model.

4.2. Energy response

The GSC gas counter is operated at the nominal HV of 1650V, which is chosen to achieve a good position resolution. It is in the limited proportionality region where the energy-PHA relation is rather distorted. Thus, the detail calibration is necessary to construct the energy-PHA response matrix. The tests for the energy response calibration were carried out for all the flight counters using X-ray beams including fluorescence lines from various target elements placed in the X-ray generator.

Figure 8 shows the energy-PHA relation derived from the calibration-test data. It has a discontinuity at 4.7 keV for Xe L-edge. The relation is well reproduced by two expedient functions for those below and above the L-edge. The deviations between the data and the model functions are within 0.6% over the 2–23 keV band.

Figure 9 shows the obtained energy resolution against the X-ray energy and that of the theoretical limit. The measured energy resolution is 16 % (FWHM) at 6 keV. It is close to the theoretical limit in the 3–5 keV band. The difference is larger at low and high energies. At low energies, a part of the electron cloud is lost by the beryllium window. At high energies, the spatial gain non-uniformity becomes effective according to the large mean free path.

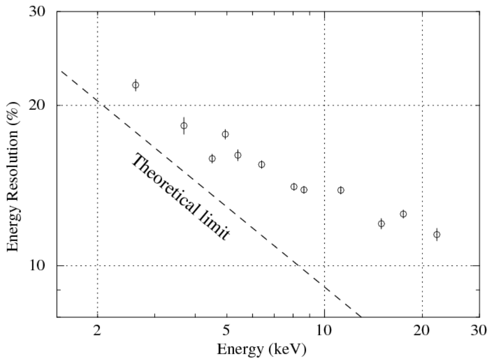

Fig. 9. Energy resolution (FWHM) against X-ray energy. Circles with 1-σ error bars represent measured data with K-shell emission lines from the elements same as those in figure 8. The theoretical limit is estimated as $2.35\{W(F+b)/E\}^{1/2}$, where the mean ionization energy $W = 21.5$ eV, the Fano-factor $F = 0.2$, and dispersion of gas gain in electron avalanche $b = 0.5$ are assumed (Knoll 1989).

4.3. Gain Spatial Non-uniformity

The gain non-uniformity along the anode wire is measured with a 2 mm pitch using Cu K_α (8.0 keV) and Mo K_α (17.5 keV) X-ray beams with a diameter of 0.2 mm. The non-uniformity among each anode cell is $\sim$ 20 % typically. The data is used in the PHA-PI conversion in the ground data reduction and also to build the energy response matrix in the spectral analysis.

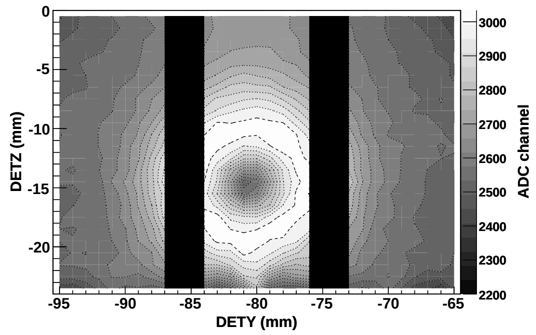

Fig. 10. Cross section of gas-gain non-uniformity in a single carbon-anode cell (C0 cell) on the plane perpendicular to the anode wire. The DETY direction is parallel to the detector window and the DETZ represent the depth from the the beryllium-window plane. The anode position is $(-80, -14.75)$. The data are obtained by the slant-beam method using X-ray beams of Mo K-line (17.5 keV). Two black stripes are unmeasurable region located under the counter-support structure. The gray scale represents the the pulse heights of the output signals for the Mo K-line.

The non-uniformity on the vertical plane to the anode wire was measured with slant X-ray beams taking an advantage of the position sensitivity. The method is described in Mihara et al. (2002). Figure 10 shows the obtained gain non-uniformity around the anode wire. The gain is the highest in the annulus of an about 5-mm

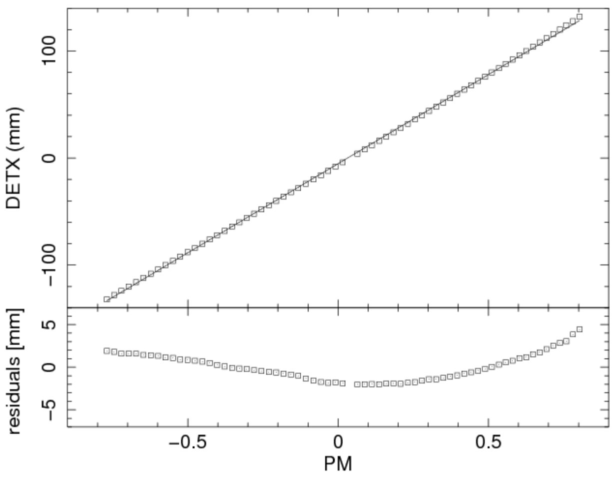

Fig. 11. Relation between the position at which X-ray is absorbed along the anode wire (DETX) and the position-measure parameter derived from the PHA ratio (PM : see text). This is for the GSC camera 6, anode 0 measured at the nominal HV of 1650 V using pencil X-ray beam of Cu K_α line . The data (square) are fitted with a linear function (solid line) in the top panel, and the residuals are shown in the bottom panel.

radius from the anode. It is lower than the average at the central region around the anode wire and the outer region. Compared to the distribution of the electric potential in figure 5, the gain has a positive correlation with the field strength in the outer region.

4.4. Position Response

Since the GSC employs slit-camera optics, the detector position response is important for determining the direction of incident X-ray photons with a good accuracy. The data of the position response is taken with a 1-mm pitch along the carbon anode using X-ray beams of Cu K-line in the ground calibration tests.

The position is encoded in the ratio of the pulse height readouts at the both anode ends. We here define the two PHA as the left $PHA_{\rm L}$ and the right $PHA_{\rm R}$ and introduce a position-measure parameter, PM,

$$PM = \frac{PHA_{\rm R} - PHA_{\rm L}}{PHA_{\rm R} + PHA_{\rm L}} \tag{1}$$

The position-measure parameter has an approximately linear relation with the event location where the X-ray is absorbed along the anode wire (figure 11). However, the relation cannot be exactly linear in the real experiment. Any analytic function cannot successfully reproduce the data obtained in the calibration tests with the required position accuracy. We thus decided to use the table-lookup method in the response function based on the ground calibration tests.

4.5. Position Resolution and High Voltage

The position resolution should be better than the slit opening width of 3.7mm to achieve the optimal angular

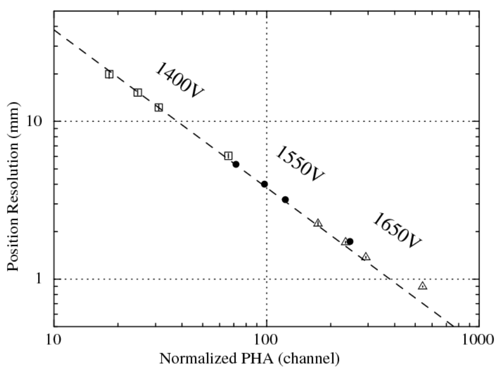

Fig. 12. Relation between position resolution (FWHM) and signal pulse height normalized by read-out amplifier gain. Squares, filled circle, and triangle points are data taken at the HV of 1400 V, 1550 V, and 1650 V, respectively. Four data points at each HV are the resolutions for Ti-K_α+K_β (4.5 keV), Fe-K_α (6.4 keV), Cu-K_α (8.0 keV) and Mo-K_α (17.5 keV). The dashed line represents an inversely proportional relation.

resolution. It is mostly determined by the ratio of the thermal noise to signal charges, which are the photoelectrons multiplied by the avalanche process in the counter.

Figure 12 shows the relation between the measured position resolution and the signal pulse height normalized by the readout-amplifier gain, obtained from data taken for X-ray beams of Ti-K_α+K_β (4.5 keV), Fe-K_α (6.4 keV), Cu-K_α (8.0 keV) and Mo-K_α (17.5 keV) in three anode voltages of 1400, 1550 and 1650 V. It is clear that the position resolution is inversely proportional to the pulse height. It is because the equivalent noise charge is constant in each anode and the position resolution depends only on the number of the multiplied signal charges. The rightmost point, measured for Mo-K_α at 1650 V, is slightly higher than the line because the mean free path of the photoelectron ($\sim$ 0.5 mm for 17.5 keV) is not negligible (Tabata et al. 1972). We determined the nominal HV of 1650 V based on the results.

References

Knoll, G. F. 1989, Radiation Detection and Measurement (Second edition) John Wiley & Sons, Inc.

Matsuoka, M. et al. 2009, PASJ , 61, 999

Mihara, T., et al., 2011, PASJ , 63, in press

Mihara, T., et al., 2002, SPIE, 4497, 173

Morii, M., Sugimori, K., & Kawai, N. 2011, Physica E: Low-dim. Systems and Nanostructures, 43, 692

Morii, M., et al., 2006, in Space Tele. and Inst. II ed. Turner, M. J. L. & Hasinger, G. SPIE, 6266, 6263U.

Shirasaki, Y., et al. 2003, PASJ , 55, 1033

Sugizaki, M., et al. 2011, PASJ , 63, in print.

Tabata, T., et al. 1972, NIMM, 103, 85

Tomida, H., et al. 2011, PASJ , 63, 395

Tsunemi, H., Tomida, H. et al. 2010, PASJ , 62, 1371